LETTERS

Assembly dynamics of microtubules at molecular resolution

Jacob W. J. Kerssemakers[1,2], E. Laura Munteanu[1], Liedewij Laan[1], Tim L. Noetzel[2], Marcel E. Janson[1,3] & Marileen Dogterom[1]

Microtubules are highly dynamic protein polymers[1] that form a crucial part of the cytoskeleton in all eukaryotic cells. Although microtubules are known to self-assemble from tubulin dimers, information on the assembly dynamics of microtubules has been limited, both *in vitro*[2,3] and *in vivo*[4,5], to measurements of average growth and shrinkage rates over several thousands of tubulin subunits. As a result there is a lack of information on the sequence of molecular events that leads to the growth and shrinkage of microtubule ends. Here we use optical tweezers to observe the assembly dynamics of individual microtubules at molecular resolution. We find that microtubules can increase their overall length almost instantaneously by amounts exceeding the size of individual dimers (8 nm). When the microtubule-associated protein XMAP215 (ref. 6) is added, this effect is markedly enhanced and fast increases in length of about 40–60 nm are observed. These observations suggest that small tubulin oligomers are able to add directly to growing microtubules and that XMAP215 speeds up microtubule growth by facilitating the addition of long oligomers. The achievement of molecular resolution on the microtubule assembly process opens the way to direct studies of the molecular mechanism by which the many recently discovered microtubule end-binding proteins regulate microtubule dynamics in living cells[7–9].

The core structure of a microtubule (MT) consists of typically 13 or 14 protofilaments forming a hollow tube (Fig. 1a). MT assembly is accompanied by the hydrolysis of tubulin-bound GTP, which occasionally triggers the MT to undergo a 'catastrophe' and switch to a state of rapid disassembly[1]. Information about the structure of growing and shrinking MT ends as well as the (preferred) conformational state of GTP-bound and GDP-bound tubulin in these situations comes from static electron microscopy studies[10–12], which indicate that growing MT ends consist of sheets of slightly outward-curved protofilaments and that shrinking MT ends consist of individual protofilaments that curve outwards more strongly.

To obtain dynamic information on the growth and shrinkage of MTs at the resolution of single tubulin dimers (8 nm) we use a technique based on optical tweezers in which we allow dynamic MT plus ends to grow and shrink against a microfabricated barrier[13]. We show results for MTs assembling from pure tubulin, and then show how, on a molecular scale, the growth process is altered by the presence of XMAP215, an evolutionarily conserved protein[14] that enhances the growth rate of MTs[15–17]. Our set-up is shown schematically in Fig. 1b (see also Supplementary Methods). MTs are nucleated by an axoneme, a naturally occurring rigid bundle of multiple stabilized MTs, to which a bead is attached near one end. The bead–axoneme construct is suspended in a 'keyhole' optical trap near a rigid, microfabricated barrier that was built into a flow cell.

The keyhole trap is used to control both the position of the bead and the direction of the axoneme. MT growth is initiated by flowing in a mixture of tubulin and GTP, with or without the addition of XMAP215. The conditions are chosen such that most of the time only one or two MTs are nucleated by the plus end of the axoneme (see Supplementary Information). When a MT reaches the barrier, further length increases lead to displacement of the bead in the trap. The relation between the increase in MT length and the displacement of the bead depends on the stiffness of the bead–axoneme construct, which we measure independently by pushing the barrier against the construct before growth is initiated. Displacement of the bead in the optical trap leads to an increasing restoring force on the bead (given by the trap stiffness k_{trap} multiplied by the bead displacement) that pushes the growing MT tip against the barrier. In all of the analysis below, we keep the growing MT short (less than 1 μm) to prevent the MT from buckling under this compressive load[18].

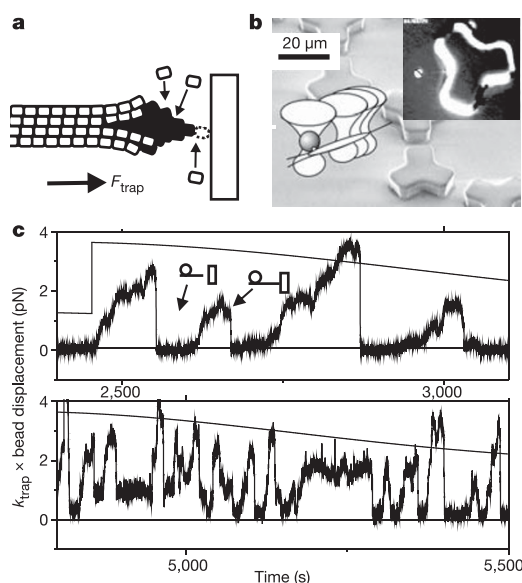Figure 1c shows the restoring force exerted by the trap during a

Figure 1 | Measuring growth dynamics of MTs with optical tweezers. a, Schematic view of a growing MT. **b**, Schematic and DIC image of a 'keyhole' optical trap holding a bead–axoneme construct in front of a microfabricated barrier. **c**, Growth and shrinkage events of individual MTs in the absence (upper panel) and presence (lower panel) of XMAP215. The smooth curves give estimates of the gradually decreasing protein concentration (maximum tubulin concentration 20 μM).

[1]Foundation for Fundamental Research on Matter (FOM) Institute for Atomic and Molecular Physics (AMOLF), Kruislaan 407, 1098 SJ Amsterdam, The Netherlands. [2]Max Planck Institute of Molecular Cell Biology and Genetics (MPI-CBG) Dresden, Pfotenhauerstrasse 108, 01307 Dresden, Germany. [3]University of Pennsylvania, Department of Cell and Developmental Biology, 421 Curie Boulevard, Philadelphia, Pennsylvania 19104-6058, USA.
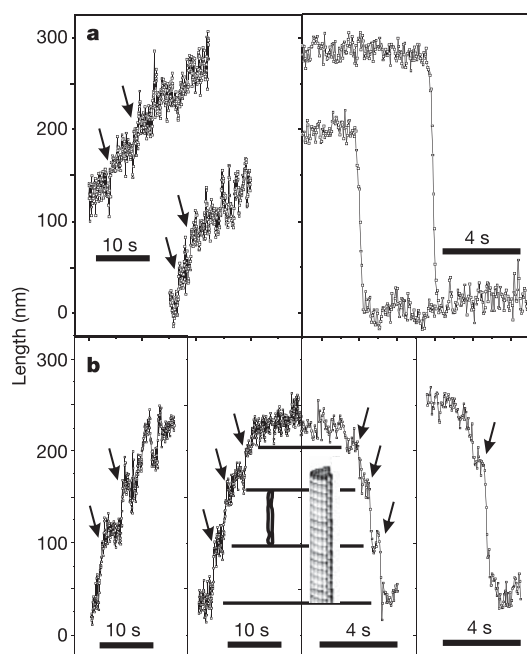
Figure 2 | **High-resolution details of growth and shrinkage events.** Length traces are shown for events without (**a**) and with (**b**) XMAP215. Arrows indicate fast length changes (steps) that are distinguishable from the noise by eye. During subsequent growth and shrinkage events in the presence of XMAP215, steps sometimes appear in register with each other (**b**, middle, lines). The insets show schematic pictures of an XMAP215 molecule (left) and a MT (right) at the same vertical scale as the length data.

comes to an apparent halt at a few piconewtons of force before catastrophes occur, which is consistent with what is known for the effect of force on the assembly dynamics of MT plus ends[18–20]. The lower panel shows growth from the same construct after replacement of the surrounding solution with 20 μM tubulin and 150 nM XMAP215. With XMAP215 present, growth is faster and catastrophes occur more frequently, in agreement with previous reports[15–17,21] and our own observations in the absence of force (Supplementary Information). The frequent occurrence of catastrophes confirms that the observed growth is that of a plus end of a MT.

Figure 2 shows part of the same data at higher resolution, this time with the MT length on the *y* axis. These data gives us unprecedented resolution on the growth dynamics of individual MTs, limited only by the thermal noise on the bead in the trap and the stiffness of the bead–axoneme construct (about 5–10 nm root-mean-square in practice). In these data we occasionally observe step-like length increases that are clearly distinguishable from the experimental noise, even by eye (Fig. 2a, arrows). When we add XMAP215 (Fig. 2b), fast increases occur more frequently and are also larger, on the order of several tens of nanometres, occurring on a timescale of about 100 ms or less (the average MT growth rate under these conditions corresponds to at most 1 or 2 nm per 100 ms). In the presence of XMAP215, steps are also clearly observed during shrinkage events (Fig. 2b, right). These steps are of similar sizes to those observed during growth, sometimes even in marked registry with previous growth steps (Fig. 2b, middle). The sizes of the large steps often seem close to the known length of the XMAP215 protein itself[22], as indicated in Fig. 2b. In addition to steps we observe periods with more gradual increases in length, in which steps are not clearly distinguishable. Given our experimental resolution this is to be expected: MT ends are likely to have multiple binding sites for tubulin dimers at unequal positions along the MT axis (see Fig. 1a), and growth due to single dimer additions, for example, should lead to mostly small steps with a maximum of 8 nm.

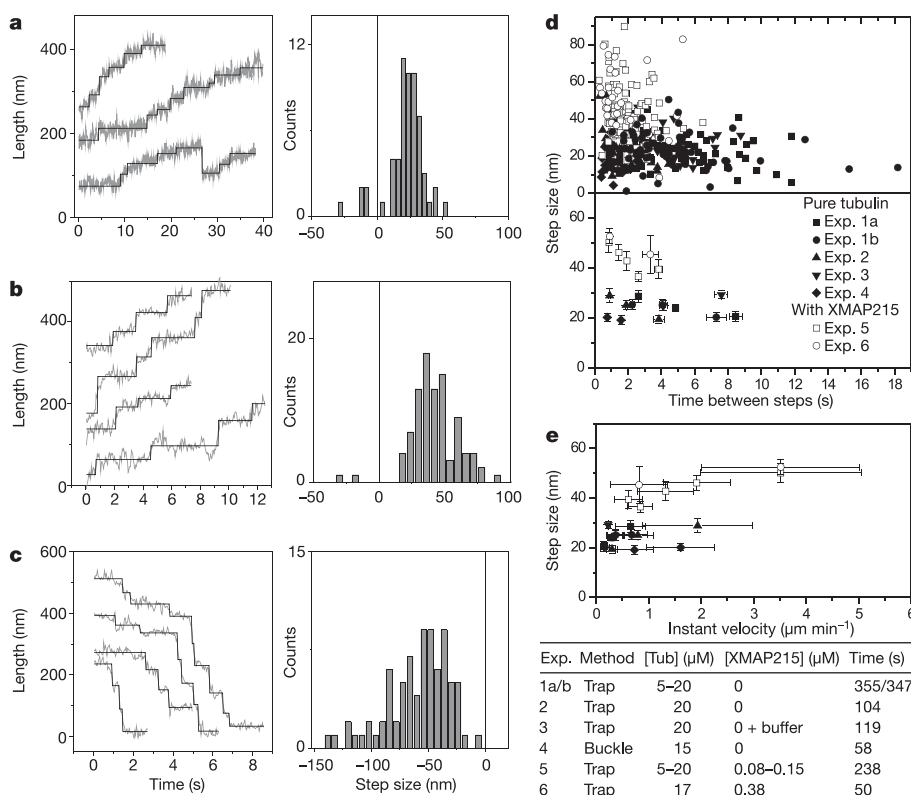To be able to analyse in an unbiased way the steps observed by eye,

sequence of MT growth and shrinkage events. The upper panel shows regular MT growth, with an initial tubulin concentration of 20 μM. The protein concentration slowly decreases as indicated by the smooth curves (as the result of a slow buffer flow). Growth often

Figure 3 | **Quantifying the sizes of the large steps with our step-fitting algorithm.** Step fits and associated step histograms are shown for regular MT growth (**a**, experiment 1a), growth with XMAP215 present (**b**, experiment 5) and shrinkage with XMAP215 present (**c**, experiment 5). **d**, Step sizes for six different growth experiments with conditions and analysed growth times as listed in the table (experiments 1a, 1b and 5 were performed with the same bead–axoneme construct; shrinkage was analysed only for experiment 5 (63 s); experiment 4 involves data obtained previously with a different 'buckling' method[20]). Top: individual step sizes plotted against the time between steps. Bottom: the same data averaged over 20 steps (the last data point may contain fewer steps). **e**, Averaged step sizes as in **d** but plotted against 'instant velocity' (step size divided by time between steps). Error bars in **d** and **e** represent s.e.m.

Exp.	Method	[Tub] (μM)	[XMAP215] (μM)	Time (s)
1a/b	Trap	5–20	0	355/347
2	Trap	20	0	104
3	Trap	20	0 + buffer	119
4	Buckle	15	0	58
5	Trap	5–20	0.08–0.15	238
6	Trap	17	0.38	50

we developed a step-fitting algorithm as outlined in the Supplementary Methods. Because in our system many of the steps were smaller than the noise, we could use the algorithm only to find and quantify the largest steps (Fig. 3). In the histograms presented, any steps (or lack thereof) close to or below the noise level are therefore insignificant. For pure tubulin growth, the step fit result and the associated histogram (Fig. 3a) confirm the presence of steps up to 20–30 nm in size. This is significantly larger than the tubulin dimer size of 8 nm. In the presence of XMAP215, the histograms for growth (Fig. 3b) and shrinkage (Fig. 3c) show larger step-like changes, around 40–60 nm in size. The observed step sizes are independent of how quickly steps follow each other (that is, the rate at which MTs grow). Our experiments were performed at various tubulin concentrations and forces (both of which affect the average MT growth velocity[20]), as well as for two different XMAP215/tubulin ratios. When we plot individual (Fig. 3d, top) and averaged (Fig. 3d, bottom) step sizes as a function of the time between steps for six different experiments (see the table in Fig. 3e), we find that the step sizes are always larger in the presence of XMAP215, even when the resulting (instant) growth velocity is the same (plotted in Fig. 3e).

The observation of fast increases in length larger than the dimer size might have two interpretations: either we were observing extended closure events of outward-curved sheets existing at the ends of growing MTs, or we were observing the addition of tubulin oligomers larger than individual tubulin dimers. To estimate the expected length increase in these two cases, we must consider the geometry and rigidity of tubulin oligomers and MT sheets as well as

the distortions that one expects in the presence of a few piconewtons of force. In our experiments MTs grew relatively slowly and never very long (typically a few hundred nanometres). In Fig. 4a we show schematically a reasonable estimate, based on electron microscopy studies[10,23], of a typical MT sheet under these conditions, drawn to scale. The estimates shown in Fig. 4 (see also Supplementary Methods) indicate that length increases due to oligomer addition, as opposed to sheet closure events, should be readily detectable.

Our observations therefore indicate that MT assembly might not always occur simply by the addition of individual tubulin dimers. Rather, small oligomers of up to three tubulin dimers seem to be able to attach to growing MTs as well. This is consistent with observations that MT assembly is reduced when tubulin oligomers are centrifuged away from MT polymerization solutions[12]. The step sizes of 40–60 nm in the presence of XMAP215 indicate that XMAP215 might facilitate the addition of even longer oligomers. Again, there are two ways in which this could be accomplished[24,25]. First, XMAP215 could template the assembly of a tubulin oligomer in solution and this whole complex could subsequently attach to the end of the growing MT (Fig. 4b, top). Because the overall growth velocity of MTs is enhanced by the addition of even a small amount of XMAP215, this would have to mean that the XMAP215–tubulin complex has a higher affinity for the MT end than tubulin alone (possibly because of 'pre-straightening' of the tubulin oligomer by the XMAP215 molecule). To us, this seems a likely mechanism because it is known from electron microscopy studies that XMAP215 can bind free tubulin dimers in a protofilament-like fashion, resulting in XMAP215–tubulin complexes with lengths up to 60 nm (ref. 22). In addition, there is indirect evidence that other MT-binding proteins such as CLIP170 bind tubulin dimers before attaching to growing MTs as well[26–28].

The second possibility is that XMAP215 could first bind to the MT end and then accelerate the build-up of an oligomer along the length of the XMAP215 molecule (Fig. 4b, bottom). In both cases it is possible that the XMAP215–tubulin complex first binds under an angle to the MT end and then straightens out the longitudinal bond in some kind of power stroke. In fact, the instant straight addition of an oligomer 40–60 nm long through a purely brownian ratchet mechanism would require an unusually large fluctuation of the MT end away from the barrier[20]. Finally, the step-like nature of shrinkage events indicates that XMAP215 might stay attached to the MT lattice for at least some time after arrival.

The method described here for detecting the molecular details of MT growth also paves the way for understanding the action of other classes of MT-associated proteins[7–9]. MT-associated proteins and end-binding proteins mediate the interaction of MTs with cellular targets such as the kinetochore and the cell cortex. Understanding, at a molecular level, the operating principles of these proteins will be essential for understanding the regulation of MT dynamics in cells.

Figure 4 | MT end mechanics. a, Schematic drawing of a MT end under a compressive force (roughly to scale). Top: a MT with a sheet-like extension of 125 nm (preferred radius of curvature $R_0 \approx 250$ nm) adopts a force-induced radius of curvature $R_F \approx 200$ nm under a compressive force of 2.5 pN (conservative estimate of the sheet stiffness 1.2×10^5 pN nm^2; that is, about 1/100 that of a MT). Middle: the same MT appears about 8 nm longer (ΔL_1) on full sheet closure. Bottom: the addition of a single, 60-nm-long protofilament (preferred radius of curvature 76 nm; stiffness 2.4×10^4 pN nm^2) under a similar compressive force will lead to an apparent length increase (ΔL_2) of about 50 nm ($R_F \approx 60$ nm). **b**, Possible mechanisms for XMAP215-enhanced addition of long oligomers.

METHODS

We used an Nd:YVO$_4$ 1,064-nm laser (Spectra Physics) to trap a 'construct': a bead connected to a rigid axoneme (Fig. 1b). The laser was time-shared to create a 'keyhole' trap[13], consisting of a point trap holding the bead and a line trap directing the axoneme towards a microfabricated barrier. Tests and calibrations of this set-up are given in Supplementary Methods. Photoresist (SU-8) barriers[29] were made by using standard microlithography techniques. Purified tubulin was obtained from Cytoskeleton Inc. and experiments were performed at 25 °C (details are provided in Supplementary Methods). Recombinant XMAP215 was expressed in Sf^+ insect cells, purified as described previously[17] and stored in liquid nitrogen. The protein concentration was determined with a Bradford assay and the molar extinction coefficient at 280 nm. Axonemes from sea urchin sperm were prepared by M. Footer from published protocols[30], and were bound to streptavidin-coated beads (2 μm diameter; Spherotech) by non-specific binding. Differential interference contrast (DIC) images of our experiments were recorded on DVD with a charge-coupled device camera (Kappa) and a standard DVD recorder (Philips DVD-R80). The displacement of the bead in the
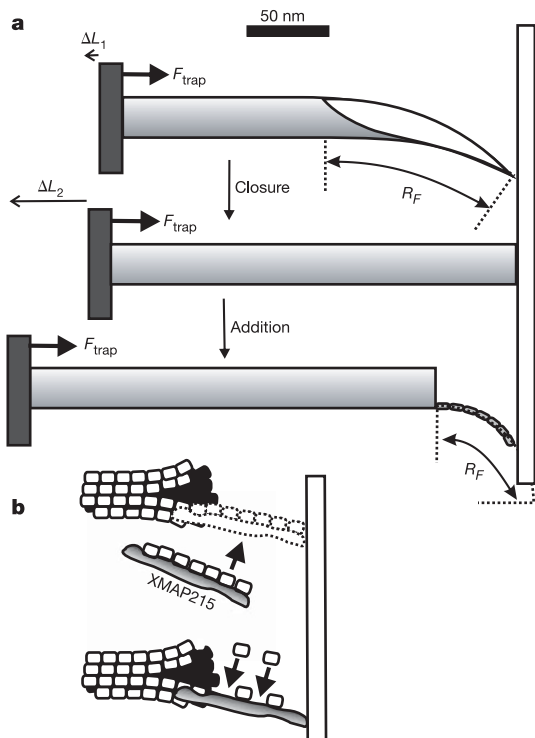
trap was measured from the digital images at a sampling rate of 25 Hz with the use of a standard auto-correlation method (image processing software home-written in IDL). A home-developed step-fitting algorithm was written in MatLab (see Supplementary Methods).

1. Desai, A. & Mitchison, T. J. Microtubule polymerization dynamics. *Annu. Rev. Cell Dev. Biol.* **13,** 83–117 (1997).
2. Walker, R. A. *et al.* Dynamic instability of individual microtubules analyzed by video light-microscopy—rate constants and transition frequencies. *J. Cell Biol.* **107,** 1437–1448 (1988).
3. Fygenson, D. K., Braun, E. & Libchaber, A. Phase diagram of microtubules. *Phys. Rev. E* **50,** 1579–1588 (1994).
4. Komarova, Y. A., Vorobjev, I. A. & Borisy, G. G. Life cycle of MTs: persistent growth in the cell interior, asymmetric transition frequencies and effects of the cell boundary. *J. Cell Sci.* **115,** 3527–3539 (2002).
5. Piehl, M. & Cassimeris, L. Organization and dynamics of growing microtubule plus ends during early mitosis. *Mol. Biol. Cell* **14,** 916–925 (2003).
6. Kinoshita, K., Habermann, B. & Hyman, A. A. XMAP215: a key component of the dynamic microtubule cytoskeleton. *Trends Cell Biol.* **12,** 267–273 (2002).
7. Schuyler, S. C. & Pellman, D. Microtubule 'plus-end-tracking proteins': the end is just the beginning. *Cell* **105,** 421–424 (2001).
8. Howard, J. & Hyman, A. A. Dynamics and mechanics of the microtubule plus end. *Nature* **422,** 753–758 (2003).
9. Akhmanova, A. & Hoogenraad, C. C. Microtubule plus-end-tracking proteins: mechanisms and functions. *Curr. Opin. Cell Biol.* **17,** 47–54 (2005).
10. Chretien, D., Fuller, S. D. & Karsenti, E. Structure of growing microtubule ends—2-dimensional sheets close into tubes at variable rates. *J. Cell Biol.* **129,** 1311–1328 (1995).
11. Wang, H.-W. & Nogales, E. Nucleotide-dependent bending flexibility of tubulin regulates microtubule assembly. *Nature* **435,** 911–915 (2005).
12. Wang, H.-W., Long, S., Finley, K. R. & Nogales, E. Assembly of GMPCPP-bound tubulin into helical ribbons and tubes and effect of colchicine. *Cell Cycle* **4,** 1157–1160 (2005).
13. Kerssemakers, J. W. J., Janson, M. E., Van der Horst, A. & Dogterom, M. Optical trap setup for measuring microtubule pushing forces. *Appl. Phys. Lett.* **83,** 4441–4443 (2003).
14. Gard, D., Becker, B. & Romney, S. MAPping the eukaryotic tree of life: Structure, function, and evolution of the MAP215/Dis1 family of microtubule-associated proteins. *Int. Rev. Cytol.* **239,** 179–272 (2004).
15. Gard, D. L. & Kirschner, M. W. A microtubule-associated protein from *Xenopus* eggs that specifically promotes assembly at the plus-end. *J. Cell Biol.* **105,** 2203–2215 (1987).
16. Vasquez, R. J., Gard, D. L. & Lynne, C. XMAP from *Xenopus* eggs promotes rapid plus end assembly of microtubules and rapid microtubule polymer turnover. *J. Cell Biol.* **127,** 985–993 (1994).
17. Kinoshita, K., Arnal, I., Desai, A., Drechsel, D. N. & Hyman, A. A. Reconstitution of physiological microtubule dynamics using purified components. *Science* **294,** 1340–1343 (2001).
18. Dogterom, M. & Yurke, B. Measurement of the force-velocity relation for growing microtubules. *Science* **278,** 856–860 (1997).
19. Janson, M. E., de Dood, M. E. & Dogterom, M. Dynamic instability of microtubules is regulated by force. *J. Cell Biol.* **161,** 1029–1034 (2003).
20. Janson, M. E. & Dogterom, M. Scaling of microtubule force–velocity curves obtained at different tubulin concentrations. *Phys. Rev. Lett.* **92,** 248101 (2004).
21. Shirasu-Hiza, M., Coughlin, P. & Mitchison, T. Identification of XMAP215 as a microtubule-destabilizing factor in *Xenopus* egg extract by biochemical purification. *J. Cell Biol.* **161,** 349–358 (2003).
22. Cassimeris, L., Gard, D., Tran, P. T. & Erickson, H. P. XMAP215 is a long thin molecule that does not increase microtubule stiffness. *J. Cell Sci.* **114,** 3025–3033 (2001).
23. Janosi, I. M., Chretien, D. & Flyvberg, H. Modeling elastic properties of microtubule tips and walls. *Eur. Biophys. J.* **27,** 501–513 (1998).
24. Spittle, C., Charrasse, S., Larroque, C. & Cassimeris, L. The interaction of TOGp with microtubules and tubulin. *J. Biol. Chem.* **275,** 20748–20753 (2000).
25. VanBuren, V., Cassimeris, L. & Odde, D. J. A mechanochemical model of microtubule structure and self-assembly kinetics. *Biophys. J.* **89,** 2911–2926 (2005).
26. Diamantopoulos, G. S. *et al.* Dynamic localization of CLIP-170 to microtubule plus ends is coupled to microtubule assembly. *J. Cell Biol.* **144,** 99–112 (1999).
27. Arnal, I., Heichette, C., Diamantopoulos, G. S. & Chretien, D. CLIP-170/tubulin-curved oligomers coassemble at microtubule ends and promote rescues. *Curr. Biol.* **14,** 2086–2095 (2004).
28. Folker, E. S., Baker, B. M. & Goodson, H. V. Interactions between CLIP-170, tubulin, and microtubules: implications for the mechanism of CLIP-170 plus-end tracking behaviour. *Mol. Biol. Cell* **16,** 5373–5384 (2005).
29. Schek, H. T. III & Hunt, A. J. Micropatterned structures for studying the mechanics of biological polymers. *Biomed. Microdevices* **7,** 41–46 (2005).
30. Pierce, D. W. & Vale, R. D. Assaying processive movement of kinesin by fluorescence microscopy. *Methods. Enzymol.* **298,** 154–171 (1998).